Perhaps the most difficult curve to desmear is the curve generated by a sphere of uniform electron density. The curve consists of a series of maxima and minima with the intensity rising and falling by many factors of ten in small intervals of h. The curve shown in Fig. 3 was smeared, and later desmeared, using a Gaussian height weighting function which fell to $1/e$ at $\pm 0{\cdot}30$ Å^{-1} and neglecting the width corrections. Since $0{\cdot}30$ Å^{-1} encompassed two secondary peaks this was felt to correspond as closely as was practical to infinite slit height smearing. The results are shown in Fig. 3. The differences between I_0 and I_{4T} are less than one per cent at the points near the peaks but still almost five hundred per cent at the calculated points near the local minima. Nevertheless, the differences would be barely observable experimentally, if at all. If we smeared and desmeared this same sphere scattering function using a height weighting function which fell to $1/e$ at $\pm 0{\cdot}075$ Å^{-1} then the errors at all calculated points, including the local minima, were less than one per cent after four iterations.

It should be noted that this method is not limited to solving the small-angle X-ray collimation equation. The author first derived it in order to correct the X-ray scattering curves for the effect of non-monochromaticity of the incident beam. Ergun (1966) has independently used equation (2) to unfold the convolution equation. Provided that a unique solution exists, it seems that the method can be applied to the solution of any integral equation of the form

$$I_{0S}(x)=\int_{-\infty}^{+\infty}\int_{-\infty}^{+\infty}\cdots\int_{-\infty}^{+\infty} W(y_1,y_2,\ldots,y_n)\, I_0[f(y_1,y_2,\ldots,y_n,x)]dy_1dy_2\ldots dy_n$$

where W is the appropriate weighting function and f is a function of $y_1,y_2,\ldots,y_n$ and x. One such equation which might be of interest is the general (*i.e.* $\sin\theta$ is not necessarily equal to θ) X-ray slit-smearing equation.

Programs can be made available on request by writing to Dr W. W. Beeman, Biophysics Laboratory, University of Wisconsin, Madison, Wisconsin.

The author would like to express his thanks to Professors Anderegg and Beeman for their helpful discussions and encouragement.

This research has been supported by research and training grants from the National Institutes of Health.

References

Chu, B. & Tan Creti, D. M. (1964). *Acta Cryst.* **18**, 1083.
DuMond, J. W. M. (1947). *Phys. Rev.* **72**, 83.
Ergun, S. (1966). Presented at the Pittsburgh Diffraction Conference, November 1966.
Guinier, A. & Fournet, G. (1947). *J. Phys. Radium*, **8**, 345.
Heine, S. & Roppert, J. (1962). *Acta Phys. Austriaca*, **15**, 148.
Kent, P. & Brumberger, H. (1964). *Acta Physica Austriaca*, **17**, 263.
Kratky, O., Porod, G. & Kahovec, L. (1951). *Z. Elektrochem.* **55**, 53.
Mazur, J. & Wims, A. M. (1967). *J. Res. Nat. Bur. Stands.* In the press.
Schmidt, P. W. & Hight, R. (1960). *Acta Cryst.* **13**, 480.
Schmidt, P. W. (1965). *Acta Cryst.* **19**, 938.

Acta Cryst. (1967). **23**, 194

Design Principles of X-ray Diffraction Cameras Linear in $f(\theta)$

By Osvald Knop
Department of Chemistry, Dalhousie University, Halifax, N.S., Canada

and A. E. Cook and F. Jackson
Nova Scotia Technical College, Halifax, N.S., Canada

(*Received* 15 *August* 1966)

The problem of designing an X-ray diffraction camera linear in an arbitrary function $f(\theta)$ of the Bragg angle is considered. While a general solution determining the shape has not been found, the complete solution for $f=k\theta$ is known, and particular solutions for $f=k\sin\theta$ and $f=k\sin^2\theta$ are given. The shape of a camera linear, along the equatorial plane, in $\sin\theta$ is an upright cardioid cylinder with the specimen at the cusp. For $f=k\sin^2\theta$ no analytic solution has been found, but perturbation and numerical methods have yielded one particular shape satisfying the condition. The practical feasibility of the cameras is discussed.

In conventional X-ray powder diffraction cameras the specimen is situated at the centre or on the circumference of a circular cylinder formed by the film. The primary beam strikes the specimen at a right angle to the cylinder axis or to a line parallel with it. The rectified length of an arc in the equatorial plane is proportional to 2θ when the specimen is at the centre (Debye–Scherrer geometry), or to 4θ when the specimen is on

the circumference (focusing geometry; the focusing effect will not be considered here). The cameras may thus be said to be linear in θ. In the following we shall consider the more general problem of cylindrical cameras linear in other functions of the Bragg angle, such as $\sin\theta$ and $\sin^2\theta$, to see what special advantages might be gained over cameras of conventional design.

The condition of linearity in $f(\theta)$, when expressed in polar coordinates, is given by

$$\int_0^{\varphi} [F^2(\varphi)+F'^2(\varphi)]^{\frac{1}{2}}d\varphi = f(\varphi/2)\,, \qquad (\theta=\varphi/2;\ f(0)=0) \quad (1)$$

where $F(\varphi)$ determines the shape of the normal cross-section of the camera; the specimen is located at the origin and assumed to behave like a point scatterer. Differentiating and squaring leads to a quadratic first-order differential equation

$$F^2(\varphi)+F'^2(\varphi)=f'^2(\varphi/2)\,. \qquad (2)$$

The solution of this equation for a general function $f(\varphi)$ does not appear to be known, even when $f(\varphi)$ is a positive monotonic increasing function, as required by the physical nature of the problem. The successive substitutions $F=f(\varphi)\,.\,\sin u(\varphi)$, $z=\tan u$ suggested by Kamke (1961) lead to Abel's differential equation

$$dz/d\varphi = \mp 1+h(\varphi)z\mp z^2+h(\varphi)z^3,\ h(\varphi)=f'(\varphi)/f(\varphi)\,,$$

which again is an equation with apparently no known solution.

However, for the special functions (1) $f(\varphi/2)=k\varphi/2$; (2) $k\sin(\varphi/2)$; and (3) $k\sin^2(\varphi/2)$ the right-hand side of equation (2) becomes respectively (1) $k^2/4$; (2) $(k^2/8)(1+\cos\varphi)$; and (3) $(k^2/4)\sin^2\varphi$, and for some of these cases particular solutions can be found. The number of solutions for a given f will depend on the continuity assumptions regarding F and F'. If F is assumed continuous, then, for any φ, $F'=\pm(f'^2-F^2)^{\frac{1}{2}}$. If the condition of continuity is imposed on both F and F' in some range including a boundary condition, there will be a unique solution for F in that range.

Case 1

The general solution of the equation $F^2+F'^2=k^2/4$ is

$$F=\pm(k/2)\{[(1-C^2)/(1+C^2)]\sin\varphi + [2C/(1+C^2)]\cos\varphi\}\,. \quad (3)$$

For $C=\cos\varphi/(1+\sin\varphi)$, $F=\pm k/2$, which is the polar equation of a circle of radius $k/2$ with centre at the origin. This corresponds to the standard Debye–Scherrer geometry, with normal incidence of the diffracted beam on the film for any φ in the equatorial plane (Fig. 1).

For fixed values of C,

$$F=\pm(k/2)(a\sin\varphi+b\cos\varphi)=\pm(k/2)\cos(\varphi-\beta)\,,$$

where $a=(1-C^2)/(1+C^2)=\sin\beta$ and $b=2C/(1+C^2)=\cos\beta$. For special choices of C one has

$C=0$	$F=\pm(k/2)\sin\varphi$
$C=1$	$F=\pm(k/2)\cos\varphi$
$C=\pm\sqrt{2}-1$	$F=\pm(k/2)[(\pm\sqrt{2}-1)/(\mp\sqrt{2}+2)](\sin\varphi+\cos\varphi)\,.$

Solutions of this type represent circles passing through the origin, with their centres displaced from $\varphi=0$ by rotation through β (Fig. 2). These cases correspond to cylindrical (focusing) cameras with the specimen at the origin, *i.e.* on the circumference of the camera. Normal incidence of the diffracted beam on the film in the equatorial plane* is obtained only for values of φ which correspond to $F(\varphi)=\max.$, *i.e.* for $\varphi=\beta$. With $C=0$ only the middle range of θ is recorded; with $C=1$, only low or high θ. For other values of C the recorded θ range varies depending on the particular choice of C. The angle of incidence in certain ranges of θ is very oblique and tends to zero as a limit.

The diffraction maxima appear at the intersections of the diffraction cones $z^2=r^2(\tan^2\alpha\cos^2\varphi-\sin^2\varphi)$ (cylindrical coordinates; equation of the cone axis, $\varphi=0$; $\alpha=2\theta=$ angle between the cone axis and the generating line passing through the origin) with the cylindrical film surfaces, $r(\varphi)=F(\varphi)$:

$$z^2=F^2(\varphi)(\tan^2\alpha\cos^2\varphi-\sin^2\varphi)\,.$$

For $F=\pm k/2$, $\varphi=\arccos\{\pm[(4z^2/k^2)+1]/(\tan^2\alpha+1)\}$. Correspondingly more complicated expressions for $\varphi(z,\alpha)$ are obtained for the other solutions. The shapes of the lines of intersection as they appear on the unrolled film are shown, at $5°\theta$ intervals, for five typical cases in Fig. 2. The back-reflection patterns ($\beta>90°$) are mirror images of the front-reflection patterns.

* Circular cylindrical coordinates, $z=0$.

† For an intensity scan in the equatorial plane using an infinitesimal aperture.

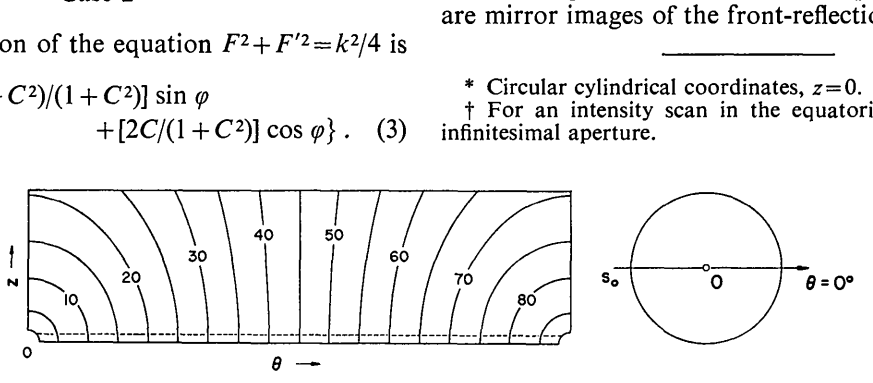

Fig. 1. Case 1, $F=k/2$: Debye–Scherrer geometry. Powder diffraction lines are shown at $5°\theta$ intervals. Broken line: the F^{-2} intensity factor.

Because the specimen-to-film distance in the peripheral mounting is not constant, an additional intensity factor $F^{-2}(\varphi)$ appears†. As a consequence, intensities in the equatorial plane will be greatly increased as the diffracted-beam vector approaches the tangent which passes through the origin.

There are no other geometries linear in θ.

Case 2

One class of solution of the equation $F^2+F'^2=(k^2/8)(1+\cos\varphi)$ is of the type $F=\pm(k/4)[1+\cos(\varphi-\beta)]$. The curve represented by F is a cardioid rotated through an angle β from $\varphi=0$, whose total length is $|2k[\cos(\beta/2)+\sin(\beta/2)]|$.

The only case of interest here is for $\beta=0$ (Fig. 3). Normal incidence in the equatorial plane obtains only at $\varphi=0$, but as this corresponds to $\alpha=0$, normal incidence exists only at one point, *viz.* $\varphi=0$, $z=0$. The shape of the lines of intersection of the diffraction cones with the surface of the cardioid cylinder is determined by the equation

$$x^4+2x^3+x^2\sin^2\alpha-2x\cos^2\alpha-[1+(4z^2/k^2)]\cos^2\alpha=0\,,$$

where $x=\cos\varphi$ (Fig. 3).

Since the line $\varphi=0$ is a tangent at the cusp, the diffraction lines are compressed in such a way that crowding occurs at high Bragg angles and the incidence in this angular range is increasingly more oblique. The intensity factor F^{-2} increases with increasing θ.

More generally, when $f(\theta)$ is a trigonometric function particular solutions of equation (1) may be obtained by a heuristic method which ultimately depends on finding an integrating factor. When equation (1) is written in the form

$$(F'+iF)(F'-iF)=fe^{i\xi}\,.\,fe^{-i\xi}\,, \qquad (4)$$

where $\xi=\xi(\varphi)$ is a function to be determined, real solu-

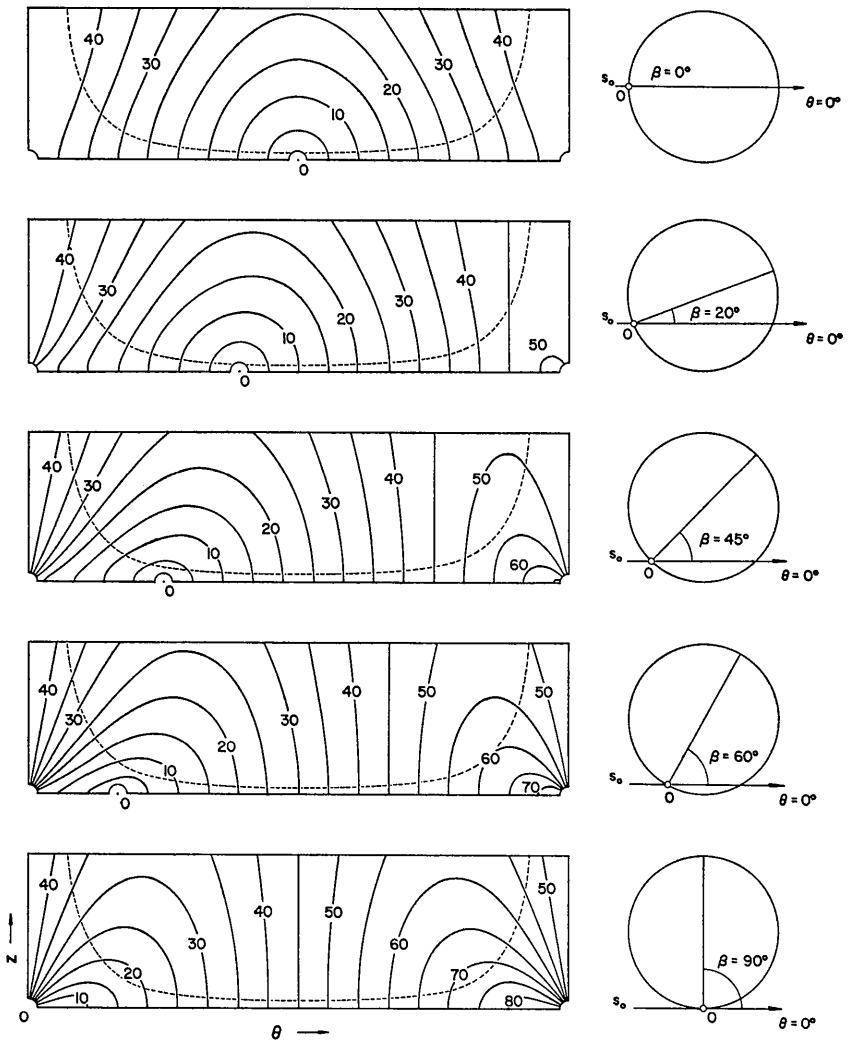

Fig. 2. Case 1, $F=(k/2)\cos(\varphi-\beta)$ (focusing geometry): Effect of β on the shape and symmetry of the powder diffraction lines. Broken lines: the F^{-2} intensity factors.

tions of the equation $F'+iF=fe^{i\xi}$ can be studied. This procedure is of no assistance in finding a general solution, since use of an integrating factor to solve the last-named equation does not lead to a useful integral equation, but many curves can be found for which the function $\xi(\varphi)$ is very simple. An example is the cardioid discussed above, for which $\tan\xi(\varphi)=-f/2f'$. Another example, not of interest in the present connection, is the n-leaved rose, $F=a\cos n\varphi$, for which $\tan\xi(\varphi)=(ff')/n^2(a^2-f^2)$.

Case 3

No analytic solution of the equation

$$F^2+F'^2=(k^2/4)\sin^2\varphi \qquad (5)$$

has been found. However, an idea of the nature of possible solutions in the real domain is gained by considering that $F^2(0)+F'^2(0)=0$. Since F and F' must be real functions of φ, the boundary conditions are $F(0)=0$ and $F'(0)=0$. Two special solutions to equation (5) are sought. In the first (case 3A), F is continuous in the range $0\leq\varphi\leq\pi$ and F' is continuous except at $\pi/2$, where $F'(\pi/2+\varepsilon)=-F'(\pi/2-\varepsilon)$. In the second (case 3B), F is continuous as in 3A and F' is continuous in some range $0\leq\varphi\leq\varphi_{\lim}$. In case 3B F will increase monotonically until F' becomes zero at $\varphi_{\lim}$; for $\varphi>\varphi_{\lim}$ F' becomes imaginary. The two solutions in F will coincide in the range $0\leq\varphi\leq\pi/2$.

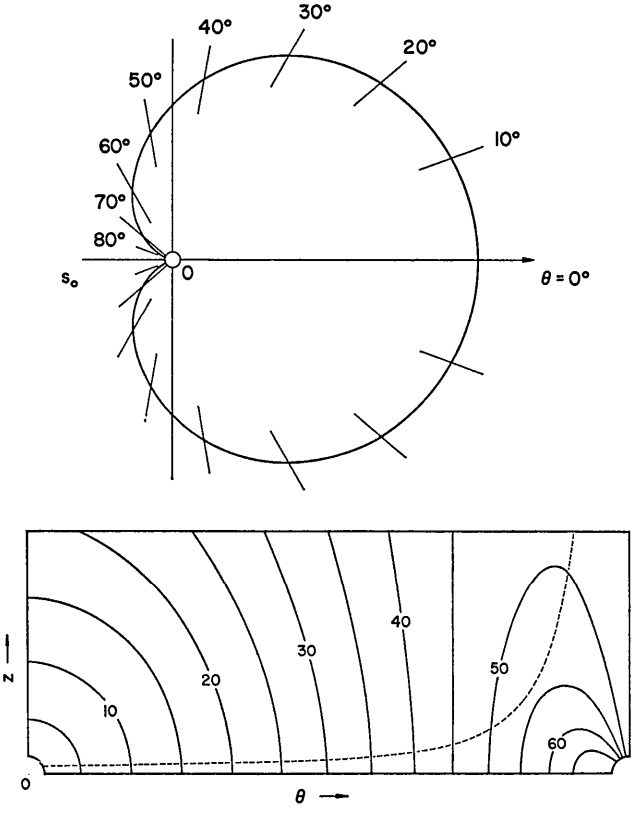

Fig. 3. Case 2, $F=(k/4)(1+\cos\varphi)$: Camera linear in $\sin\theta$.

In the following perturbation method, and in the numerical integration method, both F and F' were assumed countinous.

Equation (5) may be written as $F'^2+AF^2=(k^2/4)\sin^2\varphi$, where $F=\sum_0^\infty F_pA^p$. This leads to the following identity in like powers of A:

$$\sum_{p,q}(F'_pF'_q+AF_pF_q)A^{p+q}=(k^2/4)\sin^2\varphi \qquad p,q=0,1,2\ldots\infty . \qquad (6)$$

This identity must hold for all values of A including $A=1$. Hence equating the coefficients of A^0, A^1, A^2 *etc.* successively yields

$$\begin{aligned} F'^2_0&=(k^2/4)\sin^2\varphi \\ 2F'_0F'_1+F^2_0&=0 \\ 2F'_0F'_2+F'^2_1+2F_0F_1&=0 \\ &\vdots \\ 2F'_0F'_n+\ldots&=0 . \end{aligned} \qquad (7)$$

The formal solution $F=\sum_0^\infty F_p$, where all $F_p(0)=0$ and $F'_p(0)=0$, is obtained by setting $A=1$.

Solving equations (7), which are linear and of order one, for $n>0$ yields

$$\begin{aligned} (2/k)F_0&=2\sin^2(\varphi/2) \\ (2/k)F_1&=\sin^2(\varphi/2)-2\ln\sec(\varphi/2) \\ (2/k)F_2&=\tfrac{3}{4}\sin^2(\varphi/2)-\tfrac{1}{4}\tan^2(\varphi/2) \\ &\quad -\ln\sec(\varphi/2)+2[\ln\sec(\varphi/2)]^2 \textit{ etc.} \end{aligned}$$

Since for $n>2$ the terms of the perturbation solution become excessively complicated, the formal solution $F=\sum_0^\infty F_p$ has been truncated to $F_{\text{trunc}}=F_0+F_1+F_2=F-E$, where E is the truncation error. Direct numerical integration of equation (5) yields a solution which is in close agreement with $F-E$, thus confirming the perturbation solution; F' becomes imaginary for φ greater than $\varphi_{\lim}\simeq 1{\cdot}88$ rad, *i.e. ca.* 108°. The following values of the relative error E/F are determined by comparing F_{trunc} with F found by numerical integration:

$\varphi_{\lim}\simeq 1{\cdot}88$ rad	$E/F=6\times10^{-3}$
$\varphi=1{\cdot}5$	$E/F=5\times10^{-4}$
$\varphi=1{\cdot}0$	$E/F=4\times10^{-5}$
$\varphi=0{\cdot}5$	$E/F=1\times10^{-6}$;

thus the truncated function approximates quite closely the solution required.

The curve represented by the function $F-E$ for $0\leq\varphi\leq\pm\pi/2$ is shown in Fig. 4. In this range of φ, F is common to cases 3A and 3B. For $\varphi>\pm\pi/2$ the choice is between maximum φ coverage and absence of discontinuity in F'. In the first alternative (case 3A) the entire range $0\leq\varphi\leq\pm\pi$ is made accessible by reflecting the solution for $0\leq\varphi\leq\pm\pi/2$ in a mirror plane

passing through $\varphi = \pm\pi/2$. This solution, which is of symmetry *mm* and has discontinuities at $\pm\pi/2$, corresponds to the complete curve of Fig. 4. In the second alternative (case 3B) the curve is continued smoothly past $\pm\pi/2$ until it reaches $\pm\varphi_{\text{lim}}$. The overall symmetry of the complete solution is *m*, the mirror plane passing through $\varphi = 0$. The shape of the curve can be easily visualized by continuing the curve of Fig. 4 from $\varphi = \pm\pi/2$ to about 108°; the lines of intersection of the diffraction cones with the corresponding cylindrical surface in the range of φ between $\pm\pi/2$ and $\pm\varphi_{\text{lim}}$ do not differ greatly from those shown in Fig. 4, except that they are flatter and not symmetrical with respect to the $\theta = 45°$ line, and the vertical cut-off line is at *ca* 54°θ. The F^{-2} curve decreases steadily past the $\theta = 45°$ value.

The general case

The foregoing analysis is restricted by the initial assumption that the primary X-ray beam s_0 is perpendicular to the axis of the generalized right cylinder formed by the film, and that the film is to be measured along the trace of the equatorial plane in the cylinder surface. If these conditions are relaxed, additional configurations linear in $f(\theta)$ arise.* Some configurations would be generalized cylindrical and conical film surfaces inclined at an arbitrary angle to s_0. To achieve linearity in a specified function $f(\theta)$ the arc length could be measured, on the unrolled film, along lines other than the intersections of the equatorial plane with such surfaces. The lines could be straight or curved. No attempt will be made here to treat the general case (of which cases 1–3 are special instances), but some simple geometries suggest themselves immediately.

Let us assume that the arc length is measured along a straight line on the unrolled film, and that s_0 is always in $\varphi = 0$. The straight line can be a generating line of a cylinder or a cone and intersect s_0 at an acute angle α at a distance R from the specimen. Examples would be (*a*) a cylinder whose axis intersects s_0 at $\alpha \neq 0$; (*b*) a cone with an apical half-angle $\alpha/2$, one of whose generating lines coincides with s_0; (*c*) a cone with an apical half-angle α and the axis in s_0; and (*d*) a cylinder with its axis coinciding or parallel with s_0.

In (*a*) to (*c*), the arc length, as measured from the point of intersection of the surface with s_0, is given by $R/(\cos\alpha - \sin\alpha\cot\varphi) = (R\sin\varphi)/\sin(\alpha-\varphi)$ for the front-reflection, and by $[R\sin(\pi-\varphi)]/\sin(\alpha+\pi-\varphi)$ for the back-reflection case (observe sign of φ). For the purpose of measuring the arc length along such straight lines these (and similar) configurations can be reduced to a plane containing the straight line as a normal projection of s_0, inclined $\alpha°$ to s_0 (oblique Laue geometry). Normal Laue geometry results when $\alpha = 90°$, in which case the expression for the arc length reduces to $R/\cot\varphi = R\tan 2\theta$, and the measurement can be taken along any radius on the Laue plate.

In (*d*), $\alpha = 0$ and $R \to \infty$, so that the arc length must be measured from the point of intersection of the $\theta = 45°$ diffraction cone with the generating line most distant from s_0. When the axis of the cylinder coincides with s_0, this can be any generating line. The arc length so measured is then $\pm R\cot\varphi$, where R is the shortest specimen-to-film distance.

When the arc length is to be measured along lines other than rectilinear normal projections of s_0 on the film surfaces, a detailed investigation of the rectification properties of suitable spatial curves, and of surfaces containing such curves, would be required to find experimental arrangements that would give linearity in specified functions $f(\theta)$. This by itself might be an interesting problem in solid metric geometry.

Practical considerations (cases 1-3)

There is no difficulty in realizing the physical surfaces required in cases 1–3. Accurate machining of the cir-

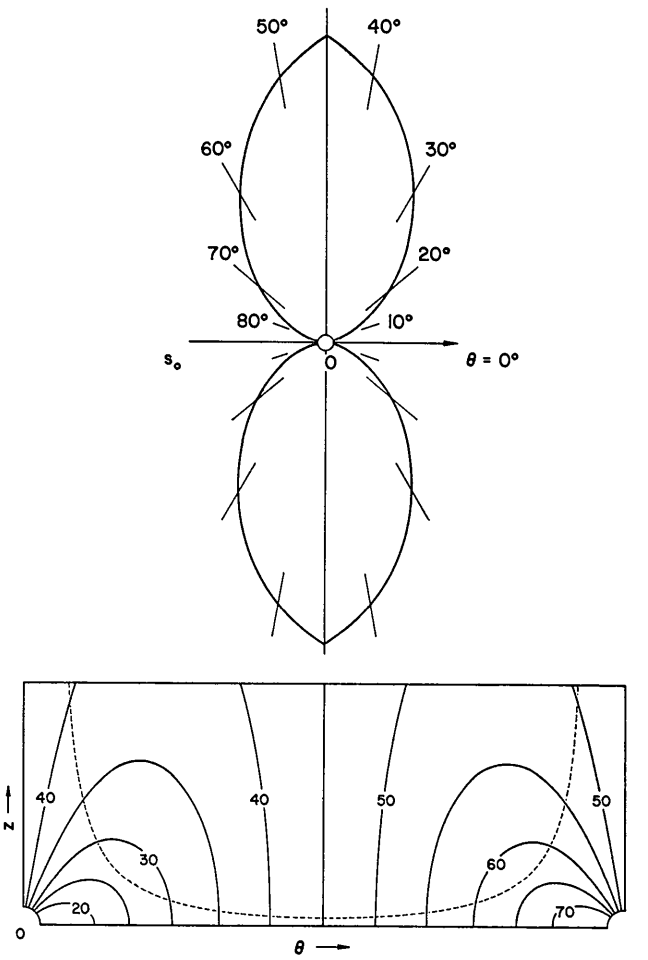

Fig. 4. Case 3: Camera linear in $\sin^2\theta$.

* The authors are indebted to the referee for pointing out the desirability of extending the original treatment of the problem to include these cases.

cular cylinders of case 1 is a trivial, if delicate, operation. The cardioid cylinder and the surfaces required in case 3 can be machined with any desired accuracy by using a computer-controlled tool.

Accurate positioning of the specimen holder presents a more difficult problem, as do the actual design of the collimator system and the termination of the machined surfaces near the specimen holder in those cases where the specimen is located on the periphery. Some of these problems and their remedies are familiar from conventional Debye–Scherrer and focusing cameras. In case 1, when $\beta \neq 0$ or 90°, a Straumanis-type film mounting is possible in principle.

In most of the cases considered, the oblique incidence of the diffracted beam, which increases the line width, imposes a severe practical limitation on the available range of θ. To minimize the increase in line width the use of single-coated film is imperative. In case 3 in particular, where there is no normal incidence, the line broadening could be prohibitive. On the other hand, in each case there is a θ range where resolution is high, and this might make some of the cameras attractive for special purposes. The possibility of direct indexing which exists with cameras linear in $\sin\theta$ and $\sin^2\theta$ might offset the disadvantages arising from oblique incidence.

In contrast to a Debye–Scherrer camera the separation of the $\alpha_1-\alpha_2$ doublets in cases 2 and 3 increases linearly: $ds/d\lambda$ varies as s/λ in case 2, and as $2s/\lambda$ in case 3 (s = length of arc in the equatorial plane). Typical values of the separation, in mm, for Cu $K\alpha$ and a film length of 180 mm (0–90°θ) would be:

θ	Debye–Scherrer	Case 2	Case 3A	Case 3B
30°	0·170	0·234	0·234	0·234
45°	0·292	0·331	0·467	0·467
85°	4·25	0·466	0·926	–

The slower increase of the separation with θ would tend to make the line crowding at high θ in case 2 and 3A less confusing, but it is doubtful whether a satisfactory resolution of the doublets could be achieved in θ ranges with pronounced oblique incidence, except perhaps with thin specimens giving very sharp lines.

Another obstacle to the practical use of non-conventional camera shapes is the coincidence of the additional intensity factor F^{-2} with the usual combined angular factor (Lorentz–polarization *etc.*) in those cases where the values of these factors separately tend, for θ approaching 0 and 90°, to increase beyond all bounds, thereby increasing the line intensities out of all proportion. Only in case 1, $\beta=0$, is there a compensation of the two factors, and in case 2 the two factors counteract each other in the low θ range.

The discontinuity at $\theta=45°$ and the location of the specimen at the origin would make it difficult to accomodate film in a camera based on case 3A. However, the angular resolution is highest precisely in the 45°θ range, which may slightly offset the disadvantage of using separate film halves. These difficulties do not arise in case 3B, but the accessible range of θ ends at *ca* 54°. This limitation could be overcome by making the camera reversible. Front-reflection and back-reflection photographs of a specimen could be taken simply by rotating the camera through 180°. The 9° overlap on each side of $\theta=45°$ would facilitate correlation of the two photographs.

Summary

The properties of the cameras discussed in this paper can be summarized as follows.

Case 1 (*Debye–Scherrer*): Circular cylinder, specimen on cylinder axis (Fig. 1). Normal incidence of the diffracted beam obtains everywhere in the equatorial plane. Doublet separation increases non-linearly with θ. F^{-2} factor is constant.

Case 1 (*focusing*): Circular cylinder, specimen on periphery (Fig. 2). Normal incidence only at $\theta=\beta/2$. When $\beta=0$ the F^{-2} factor counteracts the combined angular factor. Only one half of the total θ range is accessible when $\beta=0$. For $\beta=90°$ the geometrical coverage is from $\theta=0$ to 90°, but the practical coverage is less. F^{-2} factor depends strongly on θ.

Case 2 (*linear in* $\sin\theta$): Cardioid cylinder, specimen at the cusp (Fig. 3). Normal incidence only at $\theta=0$. Severe line crowding at high θ. High θ not accessible because of specimen holder. Maximum resolution at low θ. F^{-2} factor counteracts the combined angular factor at low θ. Doublet separation increases linearly with arc length, *i.e.* with $\sin\theta$.

Case 3A (*linear in* $\sin^2\theta$): Cylinder of a special cross-section, specimen at the origin, discontinuity at $\theta=45°$ (Fig. 4). No normal incidence. Severe line crowding at low and high θ. Very low and very high θ not accessible because of specimen holder. Maximum resolution at $\theta=45°$. F^{-2} factor reinforces the combined angular factor. Doublet separation increases linearly with arc length, *i.e.* with $\sin^2\theta$. Film would have to consist of two symmetrical sections, each covering one half of the total θ range.

Case 3B (*linear in* $\sin^2\theta$): Similar to case 3A but no discontinuity at $\theta=45°$. The cylindrical surface terminates at $\theta_{\lim}=ca$ 54°. No normal incidence. Maximum resolution at $\theta_{\lim}$. The full θ range can be made accessible by reversing the camera and taking a back-reflection photograph.

General case: The simple geometries discussed above are reducible to oblique or normal Laue cases. They would be experimentally convenient, but they do not yield arc length linear in functions of θ that can be related to the Bragg equation in a useful manner.

The Debye–Scherrer geometry is, by virtue of its symmetry, the simplest and most practical basis for the construction of an X-ray diffraction camera. Any

departure from this geometry complicates the execution and operation of the camera, so that an unconventional camera design can be justified only by the special advantages it offers. Cameras linear in $\sin\theta$ or $\sin^2\theta$ have the important advantage of making possible, at least in principle, indexing by inspection, but this advantage is gained at the expense of simplicity of design and is counteracted by certain unfavourable factors. In circumstances where the Debye–Scherrer camera is not completely satisfactory the non-standard camera could be a desirable alternative. However, one should always consider the desirable special features of non-standard cameras in conjunction with the extent of normal incidence, film utilization and coverage, the F^{-2} factor, and the extent and location of the range of maximum resolution in θ.

Reference

KAMKE, E. (1961). *Differentialgleichungen*. Leipzig: Akademische Verlagsgesellschaft.

Acta Cryst. (1967). **23**, 200

The Intensity of X-rays Diffracted by Monodimensionally Disordered Structures. Case of Identical Layers and Three Different Translation Vectors

BY M. CESARI

Società Nazionale Anonima Metanodotti, Div. LRSR, San Donato, Milano, Italy

AND G. ALLEGRA

Istituto di Chimica Industriale del Politecnico, Milano, and Centro Nazionale di Chimica delle Macromolecole del C.N.R., Sez. I, *Milano, Italy*

(*Received* 2 *July* 1965 *and in revised form* 5 *December* 1966)

The intensity of X-rays diffracted by a disordered structure in which identical layers are connected by three different translation vectors has been calculated as a function of the reciprocal vector s. The relative positions of two neighbouring layers have been supposed to exert a probabilistic influence upon the position of a third vector ($s=2$). The resulting formula may be applied to cases in which the vectors point perpendicular to the layers, as well as when the vectors have non-zero components parallel to the layers themselves. Intensity fields have been calculated and discussed for structural models related to some three-component mixed layer clay minerals. The results show that the third-component effect begins to be detectable only when the corresponding percentage is about 15–20%, and that it is more evident the greater the alternation of the various interlayer vectors amongst themselves.

1. Introduction

In the study of several layer-type structures affected by monodimensional disorder, it is generally assumed, and often proved, that only two main interlayer (or translation) vectors are present in the stacking.

There are some cases, however, for which three different vectors must be taken into account: here, we wish to recall particularly the three-component interstratified clay minerals which are rather widely distributed in sedimentary rocks (Weaver, 1956; Jonas & Brown, 1959; MacEwan, Ruiz Amil & Brown, 1961). In other cases, when the interpretation of the X-ray diffracted intensity is not completely satisfied by models of structures built up by two vectors only, the presence of a third interlayer vector should be considered at least as probable.

Owing to the lack of an adequate development of theoretical calculations, the effect of a third translation vector, besides the main two, on the X-ray intensity distribution has until now not been investigated to any extent.

A general theory recently developed by one of the authors (Allegra, 1961, 1964) seems to be particularly suitable for this purpose. In fact, it differs from other general treatments (Wilson, 1942; Hendricks & Teller, 1942; Jagodzinski, 1949*a*,*b*; Kakinoki & Komura, 1954*a*,*b*) in the sense that the physico-mathematical description of a layered disordered structure is given in terms of the statistical succession of the interlayer vectors, instead of their positions in space with reference to a fixed frame. Starting from the general results of the matrix formulation of this theory, some calculations have been carried out in order to establish a formula suitable for direct numerical computation, which allows the above mentioned effect to be explored. In particular, in the present paper, the general problem of a monodimensionally disordered structure, constituted by a large number of parallel layers with the same internal structure (*i.e.* with the same layer form factor) connected by three different translation vectors, has been investigated. Furthermore, the relative positions of two adjacent layers have been assumed to exert a probabilistic influence on the relative position of the